

LETTER

Detection of Retinal Blood Vessels Based on Morphological Analysis with Multiscale Structure Elements and SVM Classification

Pil Un KIM[†], Yunjung LEE[†], Sanghyo WOO^{††}, Chulho WON^{†††}, Jin Ho CHO^{††}, Nonmembers, and Myoung Nam KIM^{††††a}, Member

SUMMARY Since retina blood vessels (RBV) are a major factor in ophthalmological diagnosis, it is essential to detect RBV from a fundus image. In this letter, we proposed the detection method of RBV using a morphological analysis and support vector machine classification. The proposed RBV detection method consists of three strategies: pre-processing, features extraction and classification. In pre-processing, noises were reduced and RBV were enhanced by anisotropic diffusion filtering and illumination equalization. Features were extracted by using the image intensity and morphology of RBV. And a support vector machine (SVM) classification algorithm was used to detect RBV. The proposed RBV detection method was simulated and validated by using the DRIVE database. The averages of accuracy and TPR are 0.94 and 0.78, respectively. Moreover, by comparison, we confirmed that the proposed RBV detection method detected RBV better than the recent RBV detections methods.

key words: retina vessel, vessel detection, fundus image, support vector machine, morphological feature

1. Introduction

The morphology of retina blood vessels (RBV) are one of the important indicators of ophthalmological diseases, diabetes, hypertension, and retinopathy of prematurity. Therefore, RBV detection is an essential procedure for quantitative evaluation of clinical features, effective monitoring of diseases and computer aided diagnosis (CAD) of the ophthalmology [1]. There are three basic approaches in RBV detection; image threshold method, vessel tracking method, and classification method [1]–[5].

Because the intensity difference between RBV and the background is very high in a fundus image, the image threshold method based on various operators has been adopted for detecting RBV over the past few years [1], [2]. The vessel tracking method estimates a vessel location, and then finds the optimum path suitable for a vessel profile

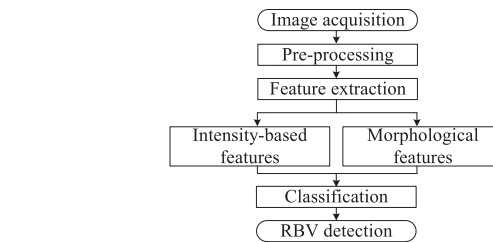


Fig. 1 Block diagram of the proposed RBV detection method.

model and criteria [3]. The classification method groups pixels or features in a fundus image into the vessel region and non-vessel region [4], [5]. Generally, it consists of 2 main stages; feature definition and classification. To define features, there are several methods such as wavelet, curvelet, 2D gabor filter, and multiscale Gaussian filter.

In this letter, we proposed a new RBV detection method by using mathematical morphology with multiscale structure elements and SVM classification. Figure 1 shows a block diagram of the proposed RBV detection method.

It consists of three strategies: pre-processing, features definition, and classification. In pre-processing, RBV are enhanced and noise is reduced by illumination equalization and anisotropic diffusion filtering. We extracted 5 intensity-based features and 12 morphological features. Finally, we employed a SVM classification algorithm.

2. The Proposed RBV Detection Method

2.1 Preprocessing

In general, a fundus image is obtained by a retina scope and image capturing equipment [2]. Mostly, the intensity of a fundus image is not uniform, because of vignetting of the lens and an unevenness of light reflecting from the fundus. Thus, we employed illumination equalization [2]. It adjusts each pixel using the following equation,

$$I_{eq}(x, y) = I(x, y) + m - \bar{I}_W(x, y) \quad (1)$$

where m is the desired average intensity, and $\bar{I}_W(x, y)$ is the mean intensity value of the pixels within a window W .

We used anisotropic diffusion filtering of Perona-Malik model to reduce noise and enhance RBV. Equation (2) is the Perona-Malik model.

$$\partial_t I = \text{div}(g(|\nabla I|^2) \cdot \nabla I) \quad (2)$$

Manuscript received October 25, 2010.

Manuscript revised March 4, 2011.

[†]The authors are with the dept. of medical & biological eng., graduate school, Kyungpook national univ., 1370 Sankyuk dong, Buk-gu, Daegu, South Korea.

^{††}The authors are with the school of electrical eng. and computer science, Kyungpook national univ., 1370 Sankyukdong, Buk-gu, Daegu, South Korea.

^{†††}The author is with the dept. of high-tech medical system, Kyungil univ., 33 Buhori Hayang Gyeongsan, Kyungpook, South Korea.

^{††††}The author is with the dept. of biomedical eng., school of medicine, Kyungpook national univ., 101 Dongindong 2 ga Jung-gu, Daegu, South Korea.

a) E-mail: kimmn@knu.ac.kr.

DOI: 10.1587/transinf.E94.D.1519

$$g(s^2) = 1/(1 + s^2/r^2) \quad (3)$$

where r is a contrast parameter separating forward (low contrast) from backward (high contrast) diffusion areas. This anisotropic diffusion filtering is a non-uniform process that reduces the diffusivity $g(s^2)$ at those locations having a larger likelihood to be edges [6]. After the illumination equalization, intensity averages of all the components approximate to m in Eq. (1). Then, the intensity of RBV is rearranged by m , and the intensity range of RBV is reduced.

2.2 Feature Extraction

First, we extracted 3 intensity-based features by the RGB components. Because the intensity difference between RBV and non-RBV is lower in red and blue components than in green components, the intensity averages of RBV and non-RBV are similar in red and blue. However, in case of the green component, the difference of each average is relatively higher than the others. Based on these characteristics of RBV color components, 3 features ($F_1 \sim F_3$) are defined by the following equations;

$$F_1(x, y) = \hat{I}_G(x, y) + m_G \quad (4)$$

$$F_2(x, y) = (\hat{I}_R(x, y) - \hat{I}_G(x, y))/(m_G/m_R) \quad (5)$$

$$F_3(x, y) = (\hat{I}_B(x, y) - \hat{I}_G(x, y))/(m_G/m_B) \quad (6)$$

where \hat{I}_R , \hat{I}_G , and \hat{I}_B are the pre-processed images of RGB component, and m_R , m_G and m_B are intensity averages of each pre-processed image of RGB components.

Next, we extracted 8 morphological features by the morphology of RBV with multiscale structure elements. Assuming that a retina in the fundus image is a flat surface, RBV are valleys having various widths. When multiscale hemispheres are rolling on surface, the flat surface is still flat while valleys become gradually flatter because they are filled by hemispheres. Therefore, those morphological characteristics can be used with respect to RBV. To obtain morphological features, 2 multiscale structure elements are defined as

$$se_s^h(c) = \begin{cases} -\sqrt{s^2 - |c|^2}, & |c| \leq s \\ 0, & |c| > s \end{cases} \quad (0 \leq c \leq s) \quad (7)$$

$$se_s^d(c) = \begin{cases} 1, & |c| \leq s \\ 0, & |c| > s \end{cases} \quad (0 \leq c \leq s) \quad (8)$$

where, c is (x, y) , and s is a constant to control the scale of the multiscale structure elements. se_s^h is a hemisphere where the radius is s . se_s^d is a circle where the radius is s , and it is used to interpolate the morphology features.

We used partial derivative of the closing operation with se_s^h to extract the morphological features of RBV. The closing operation $\phi^{se_s^h}$ is obtained by Eq. (11)

$$[\delta^{se_s^h}(f)](c) = \max_{b \in se_s^h} f(c + b) \quad (9)$$

$$[\varepsilon^{se_s^h}(f)](c) = \min_{b \in se_s^h} f(c + b) \quad (10)$$

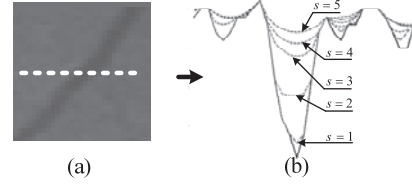


Fig. 2 (a) a sample of RBV, (b) the $\phi^{se_s^h}$ of a dash line (white), $s = [1, 5]$; solid: original image, dot: $\phi^{se_s^h}$.

$$\phi^{se_s^h}(x, y) = \varepsilon^{se_s^h}[\delta^{se_s^h}(f(x, y))], \quad 0 \leq s \leq S \quad (11)$$

And then, partial derivative of $\phi^{se_s^h}$ for s , Φ^{se^h} , can be obtained by

$$\Phi^{se^h}(x, y, s) = d\phi^{se_s^h}(x, y)/ds \quad (12)$$

Figure 2 (a) is a sample of RBV image. Figure 2 (b) shows the $\phi^{se_s^h}$ of a dash line (white) in Fig. 2 (a).

As shown in Fig. 2 (b), concavities were efficiently filled, but convexes were not changed. Thus, we used a summation of Φ^{se^h} to extract the morphological feature vsI . It defined by following equation;

$$vsI(x, y) = \sum_{s=1}^S \Phi^{se^h}(x, y, s) \quad (13)$$

And then, we extracted F_4 by

$$F_4(x, y) = \begin{cases} vsI(x, y), & vsI(x, y) > 0 \\ 0, & vsI(x, y) \leq 0 \end{cases} \quad (14)$$

Additionally, to extract 3 features ($F_5 \sim F_7$), we used maximum, mean, and standard deviation of Φ^{se^h} in the scale range. According to [1], RBV are affected by light scattering from red blood cells of fundus, when a fundus image is acquired using equipment. Thus, the thick RBV is generally darker than the thin one. For this reason, Φ^{se^h} was normalized by

$$\hat{\Phi}^{se^h}(x, y, s) = \Phi^{se^h}(x, y, s)/s \quad (15)$$

The features ($F_5 \sim F_7$) were extracted by using maximum, mean and standard deviation of $\hat{\Phi}^{se^h}$ where $0 \leq s \leq S$.

As previously stated, the intensity of RBV is affected by the red blood cells. However, as shown in Fig. 2 (a), the center line of RBV is less affected than the boundary of RBV. Therefore, we eroded $\Phi^{se^h}(x, y, s)$ with se_{s-1}^d to use variations of the center of RBV. F_8 was extracted by

$$vsI_{cen}(x, y) = \sum_{s=1}^S \varepsilon^{se_{s-1}^d}(\Phi^{se^h}(x, y, s)) \quad (16)$$

$$F_8(x, y) = \begin{cases} vsI_{cen}(x, y), & vsI_{cen}(x, y) > 0 \\ 0, & vsI_{cen}(x, y) \leq 0 \end{cases} \quad (17)$$

And, the 3 features ($F_9 \sim F_{11}$) were extracted by same method of the features ($F_5 \sim F_7$) based on Eq. (18).

$$\hat{\Phi}_{cen}^{se^h}(x, y, s) = \varepsilon^{se_{s-1}^d}(\hat{\Phi}^{se^h}(x, y, s)/s) \quad (18)$$

Lastly, we extracted 6 features ($F_{12} \sim F_{17}$) by using the eigenvalues of the Hessian matrix. These features consist of 4 morphological features based on vsl and vsl_{cen} , and 2 intensity-based features based on \hat{I}_G . The Hessian matrix H of $f(x, y)$ is defined by

$$H = \begin{pmatrix} \partial_{xx}f & \partial_{xy}f \\ \partial_{yx}f & \partial_{yy}f \end{pmatrix}. \quad (19)$$

Because $\partial_{xy}f = \partial_{yx}f$, H is symmetrical with real eigenvalues (λ_1, λ_2) and orthogonal eigenvector. The eigenvalues measure convexity and concavity in the corresponding eigendirections [6]. Therefore, the Hessian matrix is widely used to search vessels in angiography [2], [6]. We extracted features (F_{12}, F_{13}) by

$$F_{12}(x, y) = \max[\lambda_1^{vsl}(x, y), \lambda_2^{vsl}(x, y)] \quad (20)$$

$$F_{13}(x, y) = \min[\lambda_1^{vsl}(x, y), \lambda_2^{vsl}(x, y)] \quad (21)$$

where $\lambda_1^{vsl}(x, y)$ and $\lambda_2^{vsl}(x, y)$ are the eigenvalues of the Hessian matrix of vsl and we extracted features ($F_{14} \sim F_{17}$) from vsl_{cen} and \hat{I}_G by using the same methods such as in Eqs. (20) and (21).

2.3 Classification Based on SVM

Support vector machine (SVM) is widely used in pattern recognition [4], [7]. SVM is based on the statistical learning theory and the Vapnik-Chervonenkis (VC) dimension introduced by Vladimir Vapnik and Alexey Chervonenkis [7]. It finds the best separated vectors of the hyper-plane in hyper plane of n features while maximizing the distance from two classes.

3. Experimental Result

The proposed RBV detection method is simulated by the public retina database, DRIVE. This database has a set of 40 images which are divided into a training set and a test set. The training set contains the RGB fundus image, a single manual segmentation of RBV and the field of view (FOV). In the test set, there are especially two manual segmentations; one is used as the gold standard, the other one can be used to compare computer generated segmentations with those of an independent human observer. Except for fundus images which are 24 bit RGB image, manual segmentations and FOVs of the RBV are binary.

Figure 3(a) shows the green component of a fundus image and Fig. 3(b) shows the pre-processed image where W size is 40×40 , m in Eq. (1) is 128, t in Eq. (2) is 10, and r in Eq. (3) is 1. RBV are dark tubes.

There are two kinds of noises, vignetting noise and fluctuation noise. To discuss the noise reduction, we analyzed two regions in Fig. 3(a) and (b). Figure 3(c) shows the intensity graphs of two regions. Gray and black graphs are made from Fig. 3(a) and (b), respectively. Shade areas in graphs indicate RBV. These areas were based on the gold standard in DRIVE.

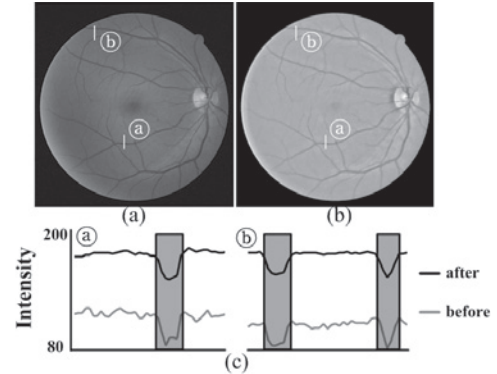


Fig. 3 (a) The green component of a fundus image, (b) the pre-processed image, and (c) image intensity graphs of ① and ②.

Table 1 Means of graphs for ① and ②.

	①	②	①-②
Fig.3(a) RBV	91	87	4
Fig.3(a) background	115	105	10
Fig.3(b) RBV	155	154	1
Fig.3(b) background	178	177	1

Table 2 Standard deviation of graphs for ① and ②.

	Fig.3(a)	Fig.3(b)	Fig.3(b)-Fig.3(a)
RBV	①	4.2	2.7
	②	4.0	2.7
background	①	3.2	2.4
	②	2.8	2.6

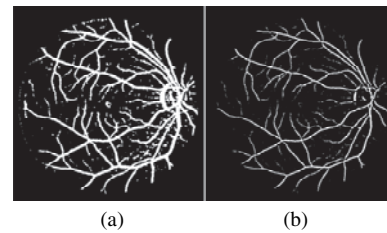


Fig. 4 Results of Eq. (13) and (16); (a) vsl (b) vsl_{cen} .

Table 1 shows means of two regions. As shown in Table 1, the absolute difference between means of RBV ① and ② is 4 in Fig. 3(a). After pre-processing (Fig. 3(b)), it fell to 1. In case of the background, it fell from 10 to 1. Therefore, the intensity ranges of RBV and background were reduced, which means that vignetting noise was reduced by illumination equalization.

Table 2 shows standard deviations of two regions. As shown in Table 2, the standard deviations of each graph were all reduced after pre-processing. As shown in Fig. 3(c), areas of the RBV and background were smoothed. Therefore, fluctuation noise was reduced by anisotropic diffusion filtering. However, boundaries between RBV and background are well preserved. Therefore, it was confirmed that noises were reduced and areas of RBV and background were smoothed while boundaries between RBV and background were well preserved.

Figure 4(a) and (b) show vsl and vsl_{cen} where $S =$

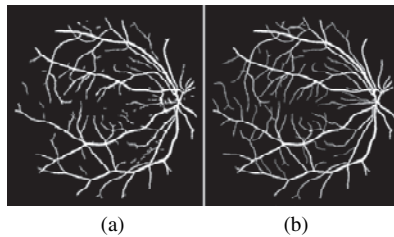


Fig. 5 RBV detection results; (a) the proposed RBV detection method, (b) a manual result.

Table 3 Comparison with other RBV detection methods.

Method	Average of TPR	Average of accuracy
2 nd manual results	0.7761	0.9473
The proposed method	0.7862	0.9492
Xu [4]	0.7760	0.9328
Mendonca [3]	0.7344	0.9452
Martinez-Perez [1]	0.7246	0.9344
Staal [5]	0.7194	0.9442

[0, 5]. Results of vs_l are thicker than ones of $vs_{l_{cen}}$. As shown in Fig. 4 (a) and (b), it is confirmed that values of the thick RBV are higher than the thin RBV.

To build a SVM classification, we gathered the training samples from 20 fundus images in the training set of DRIVE. In an image, 1,000 RBV samples and 1,000 non-RBV samples were randomly selected. So, total 40,000 training samples were used to train SVM.

Figure 5 (a) and Fig. 5 (b) show a manual result and a final result of the proposed RBV detection.

As shown in Fig. 5, the proposed RBV detection method detected mostly thick RBV.

Finally, we compared the proposed RBV method with 4 RBV detection methods. Perez, et al used the multiscale analysis with the first and second spatial derivative of a Gaussian kernel [1]. Xu, et al used RBV by SVM classification and features which were extracted by a wavelet transform and a curvelet transform [4]. Mendonca, et al used a top-hat operator and region growing [3]. Staal, et al used the line detector and k-NN classifier and sequential forward feature selection [5].

In comparison, we used true positive rate (TPR) and accuracy between the manual results and each detection results. If the detection result was completely the same as the first manual result, TPR and accuracy should be one. Table 3 shows the comparison results with a test set of DRIVE. A test set had 20 fundus images. Especially, since second man-

ual results are included in a test set, we added them in the comparison. As shown in Table 3, there are the averages of TPR and the accuracy of each RBV detection method. The results of the proposed RBV detection method were 0.78 and 0.94, respectively.

Therefore, we confirmed that the proposed RBV detection method detected RBV better than other detection methods.

4. Conclusion

RBV detection is an essential procedure in analyzing a retina for diagnosis. Thus, we proposed the novel RBV detection method by using morphological analysis and SVM classification. In the experiment, the proposed RBV method effectively detected RBV in the fundus image. By quantitative comparison, we confirmed that the proposed RBV detection method efficiently detected RBV and is better than recent methods. Therefore it is expected that the proposed RBV detection method could be widely applied in anatomical analysis; such as optic disc detection, retina mapping, and angiography.

Acknowledgements

This study was supported by a grant of the Korea Healthcare technology R&D Project, Ministry for Health, Welfare & Family Affairs, Republic of Korea.

References

- [1] M. Perez, A. Hughes, S. Thom, A. Bharath, and K. Parker, "Segmentation of blood vessels from red-free and fluorescein retinal images," *Med. Imag. Analysis*, vol.11, pp.47–61, 2007.
- [2] A. Hoover and M. Goldbaum, "Locating the optic nerve in a retinal image using the fuzzy convergence of the blood vessels," *IEEE Trans. Med. Imaging*, vol.22, no.8, pp.951–958, 2003.
- [3] A. Mendonca and A. Campilho, "Segmentation of retinal blood vessels by combining the detection of centerlines and morphological reconstruction," *IEEE Trans. Med. Imaging*, vol.25, no.9, pp.501–509, 2004.
- [4] L. Xu and S. Luo, "A novel method for blood vessel detection from retinal images," *IEEE BioMed. Eng., OnLine* 9:14, 2010.
- [5] J. Staal, M. Abramoff, M. Niemeijer, M. Viergever, and B. van Ginneken, "Ridge-based vessel segmentation in color images of the retina," *IEEE Trans. Med. Imaging*, vol.23, no.4, pp.501–509, 2004.
- [6] D. Eberly, *Ridges in Image and Data Analysis Computational Imaging and Vision*, Kluwer Academic Publishers, Netherlands, 1996.
- [7] C. Burges, *A Tutorial on Support Vector Machines for Pattern Recognition*, Bell Lab., Kluwer Academic Publishers, 1998.